Tunnelling and Underground Space Technology 86 (2019) 186–197

Contents lists available at ScienceDirect

Tunnelling and Underground Space Technology

journal homepage: www.elsevier.com/locate/tust

Study of infrared thermal application for detecting defects within tunnel lining

Alireza Afshani[a,*], Koichi Kawakami[b], Shinji Konishi[b], Hirokazu Akagi[a]

[a] Department of Civil and Environmental Engineering, Waseda University, 58-205, 3-4-1, Ohkubo, Shinjuku, Tokyo 169-8555, Japan
[b] Structural Sec. Infrastructure Maintenance Dep. Tokyo Metro Co. Ltd., 19-6 Higashiueno 3 chome, Taito-ku, Tokyo 110-8614, Japan

ARTICLE INFO

Keywords:
Infrared thermography
Defected lining
Heat transfer
RC tunnel lining
Hammering test

ABSTRACT

With the aging of tunnels, additional maintenance and assessment procedures are required to monitor their working conditions. The passive thermal infrared method, which is a nondestructive contact-free method, is used to find defects in a box-type and shield tunnels with concrete lining. In this study, this method is numerically applied to detect defects in an unhealthy concrete structure. The thermal field data measurements are reviewed and the governing heat transfer mechanisms for a defected concrete surface are presented. The heat transfer in the concrete segment, tunnel air, and the air inside the void due to the conduction, convection, and radiation mechanisms is explained. Further, the type of cavity, the temperature difference between the healthy and unhealthy concrete surfaces, the temperature difference between the tunnel air and concrete surfaces, and the influence of the void depth on the detection accuracy are investigated. The results show that the temperature difference between the concrete surface and the tunnel air is more than 0.35 °C, which is an ideal condition for detecting the voids with an approximate depth of 30 mm or less.

1. Introduction

Infrared thermal application is a nondestructive contact-free method of using infrared thermometry (IRT) to find defects in a concrete structure. However, there are limited cases wherein this method is used for void detection in tunnel linings (Konishi et al., 2016). The IRT is implemented using either active or passive methods. In active thermography, an internal or external source of heat is used to create the temperature difference between the concrete surface and the tunnel air (Danesi et al., 1998; Maierhofer et al., 2006; Sakagami and Kubo, 2002) whereas the temperature of the subjects are measured in their natural states without actively heating or cooling the surface in the passive method. In the case of active thermometry, the method is appropriate for visualizing inhomogeneity and defects close to the surface (up to a depth of 10 cm) (Maierhofer et al., 2006), and in the case of passive thermometry, the method is recommended for voids with a depth of less than 5 cm (Sakagami and Kubo, 2002). Maierhofer et al. (2004) experimentally investigated the possibility of locating defects with different sizes and depths in a concrete segment using active thermography. The experimental data were quantitatively analyzed and the effects of environmental conditions and material and geometrical parameters were demonstrated. In a new attempt, Showunmi (2013) examined the depth of the defects, temperature difference between the ambient and concrete surface, and heating duration by performing an experimental IRT test on steel–concrete composite walls, and subsequently, used numerical analyses to validate the findings. He found that the numerical method could be used to determine the correct behavior of infrared thermography; however, the accuracy was not convincing. The results of his study demonstrated that defects within the specimen were detectable at certain depths, heating intensities, and heating duration; however, the depth of the defect is one of the most evident limitations in detecting the defects on the subsurface of the specimens. In the application of passive IRT to tunneling, Konishi et al. (2016) performed several passive field IRT measurements during train non-operating hours to confirm the feasibility of applying this method to tunnels and compared the results by conducting a hammering test.

The heat in the concrete segment, tunnel air, and the air inside the void is transferred via conduction, convection, and radiation mechanisms (Guo et al., 2011; Kim et al., 2014). As the performance of infrared thermography has improved in recent years, the possibility of detecting voids has increased, even in areas of the tunnel where the variation in the temperature is small.

This study numerically modeled heat transfer in the concrete, tunnel air, and air inside the void. We verified the model by comparing it with thermal field data. The relationship was determined between the temperature difference of healthy and unhealthy concrete surfaces and the

* Corresponding author.
E-mail address: aafshani@aoni.waseda.jp (A. Afshani).

https://doi.org/10.1016/j.tust.2019.01.013
Received 12 September 2017; Received in revised form 13 July 2018; Accepted 13 January 2019

Nomenclature

List of symbols

q	transferred heat, W.m
A	area through which the heat is transferred
h	convective heat transfer coefficient, W/(m^2 K)
T_a	ambient temperature, ˚C
T_0	initial temperature, ˚C
T_s	surface temperature of cavity elements, ˚C
k	thermal conductivity, W/m K
c	specific heat, J/kg K
γ	mass density, kg/m^3
e	emissivity of the given system
σ	Stephan–Boltzmann constant, W/m^2 K^4
t_1	surface temperature of healthy concrete, ˚C
t_2	surface temperature of unhealthy concrete, ˚C
T	tunnel air temperature, ˚C

depth of the void in order to apply this method appropriately to engineering practice. This study demonstrates the accuracy of detecting non-visible voids by comparing the field measurement data with the numerical results of relevant heat transfer analyses. Further, the type of cavity, the temperature difference between the healthy and unhealthy concrete surfaces, the temperature difference between the tunnel air and the concrete surfaces, and the influence of the void depth on the detection accuracy are investigated using numerical analyses.

2. Thermal data measurement

2.1. Temperature variation in tunnel

Field thermal data measured inside of an RC-box type tunnel and a shield tunnel are explained in this part. Fig. 1 shows the application of the passive infrared thermography for an RC box-type tunnel of length 2 km. Fig. 2 shows the same for a shield tunnel (length of 100 m) with RC lining. Fig. 1 also shows a hammering test and thermal imaging locations. The temperature difference between the tunnel air and the concrete surface ($t_2 - T$) and between healthy and unhealthy concrete surfaces ($t_2 - t_1$) is important for ensuring accurate void detection. Two sets of thermal measurement data with different thermal conditions are reviewed in this section. The first dataset contains higher values of $t_2 - T$ than the second dataset. The criteria for detecting defected concrete surfaces and the application these criteria to the datasets using field data and numerical results are given in the following sections. Fig. 3(a) shows the field data pertaining to the change in the temperature of the tunnel air T, healthy concrete surface t_1 (without defect), and unhealthy concrete surface t_2 (with defect) with respect to the time of the day (24 h) measured along the RC box-type tunnel.

During the day, trains commute through the rail and the temperature inside the tunnel increases. However, the temperature decreases after mid-night because the trains do not commute (rest hours). Fig. 3(b) shows the difference in temperatures between the concrete surface and the tunnel air, i.e., $t_2 - T$, and that between the unhealthy and healthy concrete surfaces, i.e., $t_2 - t_1$, pertaining to the same data. In this set of measurement data, the difference in temperature between the tunnel air and the concrete surface is considerable—in all cases more than 0.35 ˚C. The temperature difference between the healthy and unhealthy parts of the lining is also indicated on the same graph; the temperature difference is less than 0.55 ˚C.

Fig. 4 shows another set of field data similar to that shown in Fig. 3 measured each minute over 24 h. However, in this dataset, there is relatively little difference in temperature between the tunnel air and concrete surface ($t_2 - T$). Fig. 4(a) shows the temperatures of the healthy and unhealthy concrete surfaces and the tunnel air and Fig. 4(b) shows values of $t_2 - t_1$ and $t_2 - T$ for the same data. The measurement data pertaining to t_1, and thus, $t_2 - t_1$ were available until 12 noon. According to the field measurements shown in Fig. 4(b), except for the time between approximately 7 and 9 AM, $t_2 - T$ values are less than 0.35 ˚C. The temperature difference between the healthy and unhealthy surfaces is less than 0.15 ˚C, i.e., $|t_2 - t_1| < 0.15$ ˚C. Fig. 5(a) shows the infrared image of a defected tunnel-lining surface. Fig. 5(b) shows the temperature variation along the two perpendicular lines 1 and 2. The temperature distribution near the sides of the void along line 1 is largely symmetrical; however, as the surface temperature of the concrete is higher near the tunnel crown, the temperature along the positive direction of line 2 slightly decreases. Along both the lines 1 and 2, a temperature difference of approximately 0.6 ˚C between the center and boundary of the defected area is observed.

2.2. Void detection criteria

Void detection using IRT generally depends on the temperature difference between the concrete surface and the tunnel air and the temperature difference between the healthy and unhealthy concrete surfaces. In order to determine how accurate IRT is at detecting voids, non-destructive hammering tests were performed in the same location at which IRT was performed (see Fig. 1). The hammering tests were conducted by skilled inspectors of all surfaces on a limited section of the tunnel where there was a high chance of the presence of actual voids.

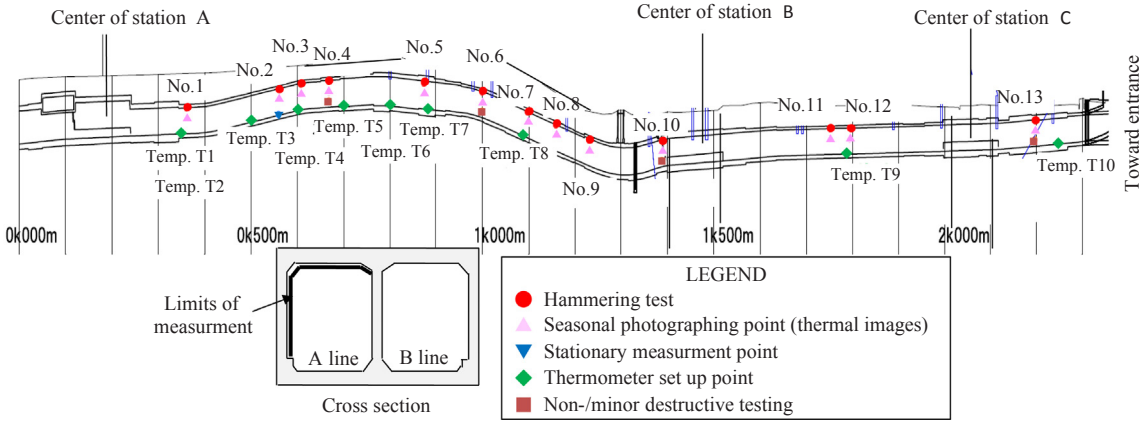

Fig. 1. Infrared thermography measurement along the RC box-type tunnel.

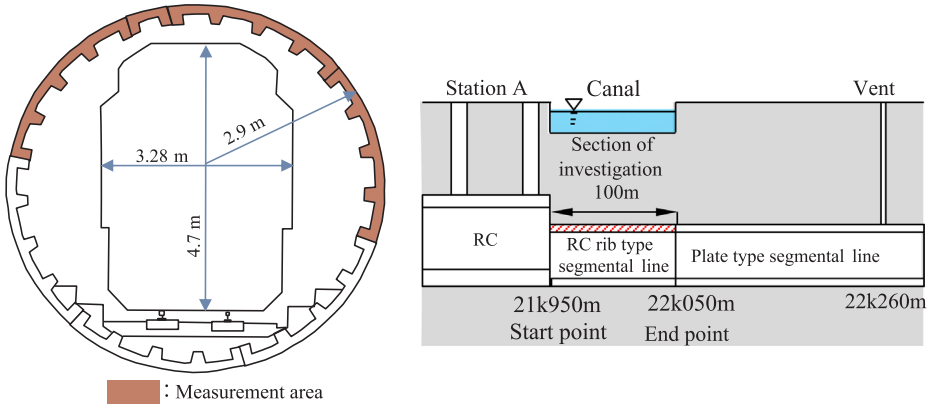

Fig. 2. Infrared thermography measurement along a shield tunnel with RC lining.

Owing to the experience of the inspectors, we can assume that the actual number of voids was very close to the number of the voids they detected from hammering tests. Indeed, for the purpose of this study, and for the sake of simplicity, we assumed that the actual number of voids was the same as those obtained by the hammering tests. The ratio of the number of voids detected by IRT to that detected by hammering tests is hereafter referred to as the void detection ratio. Fig. 6 shows the field measurement data of the void detection ratio in three cases based on the temperature difference between the concrete surface and the tunnel air. When the concrete surface temperature is lower than that of the tunnel air (Case 1: $T > t_2$, heat absorption case), the detection rate of the defects is approximately 40%, which is also the case even if the temperature difference between the concrete surface and the tunnel air is large. For the case wherein the temperature of the concrete surface exceeds that of the tunnel air (Case 2: $T < t_2$, heat radiation case), the chances of detecting the defects are high. The larger the difference in temperature, the higher is the detection rate. If the temperature difference increases beyond 0.35 °C, the detection rate is approximately 76%. For case 3, the dimensions of the voids are 10 cm × 10 cm or more, and the detection rate reaches an overall rate of 78%. The thermal camera can detect the voids when the temperature difference between the healthy and unhealthy concrete surfaces is more than 0.03 °C (regarding the camera used for data measurements). That is, the detection is feasible if $t_1 - t_2 > 0.03$ °C (Konishi et al., 2016).

Fig. 7 shows the thermal images of the RC box-type tunnel captured between November 5:26 am to 7:16 am 2013 at the section 0 km, 556 m (see Fig. 1) under the condition that the range of temperature difference between the concrete and tunnel air is 0–0.5 °C. As the temperature difference between the concrete surface and the tunnel air increases above 0.2 °C, the void detection is possible and as this number reaches

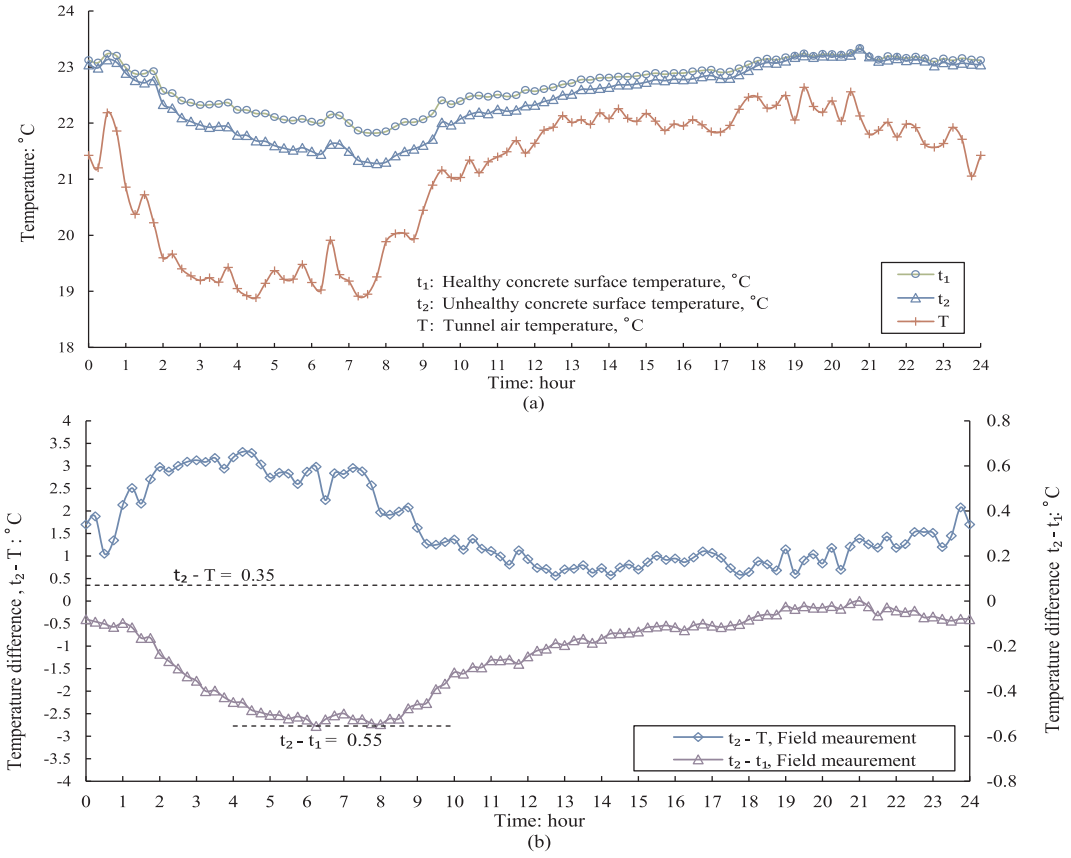

Fig. 3. Field measurements of temperature changes in the tunnel air and healthy and unhealthy concrete surfaces with respect to time (ideal condition).

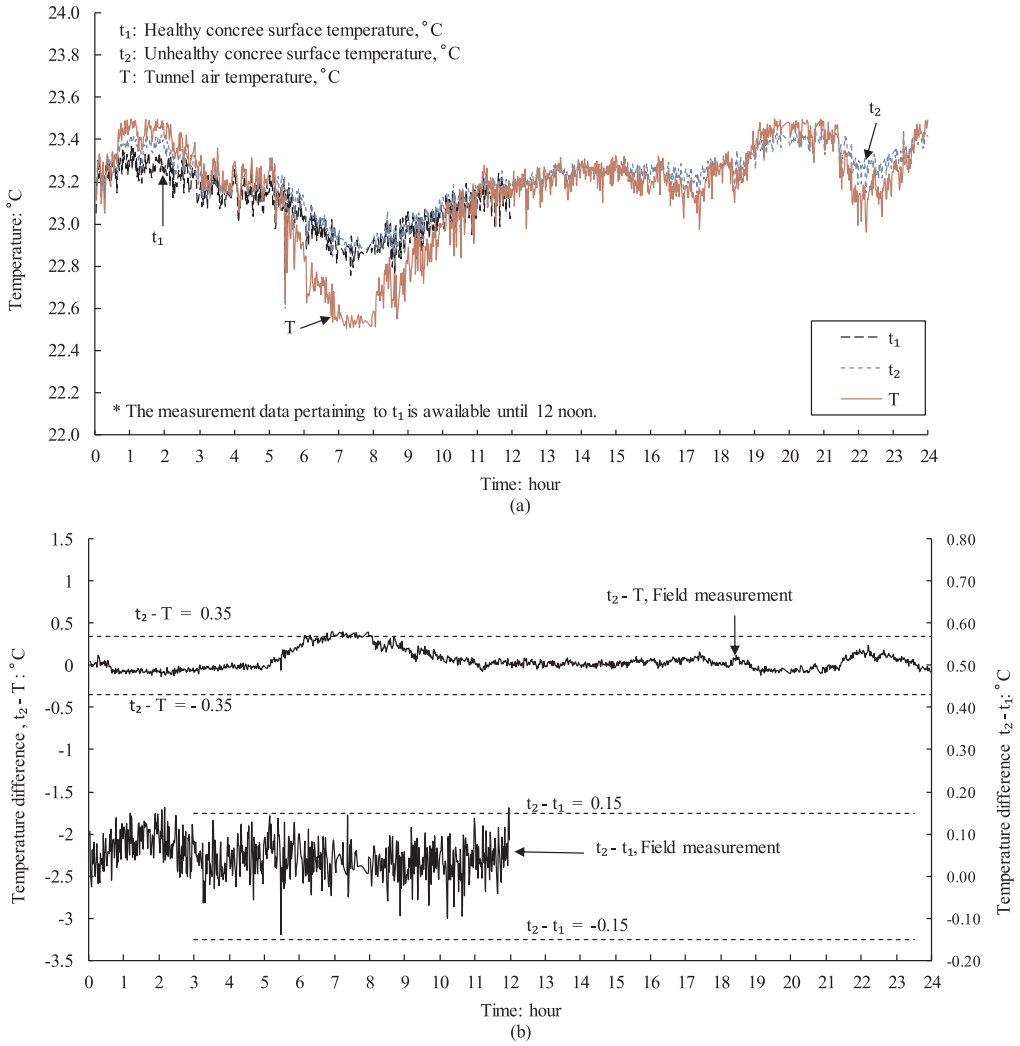

Fig. 4. Field measurements of temperature changes in the tunnel air and healthy and unhealthy concrete surfaces with respect to time (difficult condition).

0.35 °C, a clear distinction is noticeable.

3. Numerical analyses

The heat transfer in the concrete segment, tunnel air, and the air inside the void is due to conduction, convection, and radiation

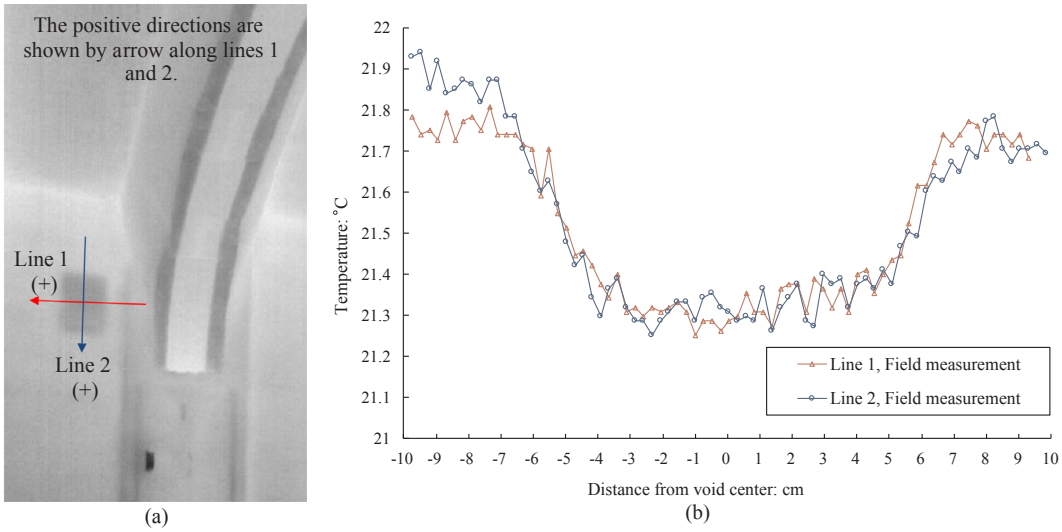

Fig. 5. (a) Infrared image of a defected concrete, and (b) temperature variation along the two perpendicular lines 1 and 2.

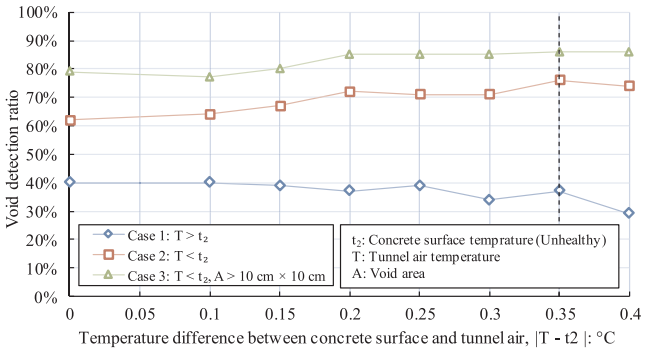

Fig. 6. Void detection ratio with respect to the temperature difference between the concrete surface and the tunnel air.

mechanisms. This issue has been addressed previously (Maierhofer et al., 2004; Scott et al., 2012; and Mahmoud et al., 2012). These mechanisms are employed in the numerical modeling of this phenomenon. The temperature difference between the healthy and unhealthy concrete surfaces, temperature difference between the tunnel air and the concrete surfaces, type of cavity, and the influence of the void depth on the detection accuracy are investigated using numerical analyses.

3.1. Heat transfer mechanisms

The heat between the concrete surface, tunnel air (ambient air), and the air inside the void is transferred as follows:

Concrete segment surface and tunnel air: Heat between the concrete surface and tunnel air is exchanged via transient heat convection mechanisms. The initial temperature of the whole concrete segment volume and the temperature changes to the concrete surface over time (T) is introduced according to the field measurement data shown in Figs. 3 and 4. The transfer of heat between the concrete surface and tunnel air by convection mechanisms is derived as follows:

$$q = -hA(T_s - T_a) \quad (1)$$

Here, q is the transferred heat (W m), h is the convective heat transfer coefficient (W/(m^2 K)), A is the area involved in the heat transfer via convection (m^2), and T_a and T_s are the ambient and surface temperatures, respectively (°C).

Concrete segment surface and soil boundary: The soil outside of the tunnel concrete lining is considered to have constant temperature regardless of depth change from the tunnel crown to the invert of most tunnels. Fluctuation in soil temperature is negligible at normal depths of most tunnels throughout the year. Kyuma (1985) measure the soil temperature at multiple stations of different depths across Japan and showed that the approximate soil temperature for a depth of more than 2 m in the area near Tokyo is between 13 °C and 19 °C. In this study, soil temperature was taken to be constant and equal to 16 °C. This value was also suggested by local IRT experts. The initial concrete segment volume temperature is introduced to the numerical model based on field measurement data. Then, the temperature at the outer concrete surface adjusts to the soil temperature via the steady-state heat convection mechanisms according to Eq. (1).

Inside the concrete segment: Assuming homogenous and isotropic material, the heat inside an undamaged concrete segment is transferred via conduction. By changing the temperature at both the outer and inner sides of concrete surfaces, the heat transfer inside the concrete is calculated according to conduction as follows:

$$q = -kA(\Delta T/\Delta n) \quad (2)$$

Here, q is the transferred heat (W m), k is the thermal conductivity (W/m K), and $\Delta T/\Delta n$ is the temperature gradient in a direction perpendicular to the area A (m^2). The temperature distribution inside the concrete is affected by the thermal properties of the material including the conductivity (k), specific heat (C), density (ρ), and thermal diffusivity (α). The transient 3D convective heat transfer for the concrete is governed by the following Fourier equation.

$$\frac{\partial T}{\partial t} = \alpha \nabla^2 T, \quad \alpha = \frac{\kappa}{\rho c} \quad (3)$$

Here, t is the time, and T is temperature.

Concrete surfaces around the void and the trapped air inside the void: As defects develop in the area near to the concrete surface, air gaps of varying sizes become trapped within the concrete. This air interacts with surfaces of the closed cavity by radiation. The theory on which cavity radiation is based is well known and can be found in Holman (1990). The application of cavity radiation to the inside surface surrounding the air void within concrete defects has also addressed in previous studies (Mydin, 2013; Showunmi, 2013). The heat transfer between surfaces of the void and trapped air is calculated as follows:

$$q = e\sigma A(T_s^4 - T_a^4) \quad (4)$$

Here, q is the heat transferred via radiation (W m), e is the emissivity of the system, σ is the Stephan–Boltzmann constant ($=5.6697 \times 10^{-8}$ W/m^2 K^4), A is the area involved in the heat transfer via radiation (m^2), and ΔT is the difference in temperature between the two systems.

3.2. Numerical model

To generate more data and better interpret the measurement data, a numerical model was employed. The numerical analyses were conducted using Midas NFX, which is a commercial software program for finite element analyses. The width, length, and thickness of the lining segment piece were 80, 100, and 30 cm, respectively. The width, length, and thickness of the cavity were 10, 10, and 0.5 cm, respectively. Assuming that the defected area is located at the center of the segment piece near the internal concrete surface, only a quarter of the concrete block is modeled, as shown in Fig. 8(a)–(c). The sides of the model are assumed adiabatic, implying that the heat is not allowed to pass through them.

The top of the lining segment piece is in contact with the soil at a constant temperature of 16 °C and loses heat via the steady convection mechanism. The internal surface of the segment exchanges heat with the tunnel air via the transient convection mechanism. The tunnel air temperature changes with respect to time based on the data shown in

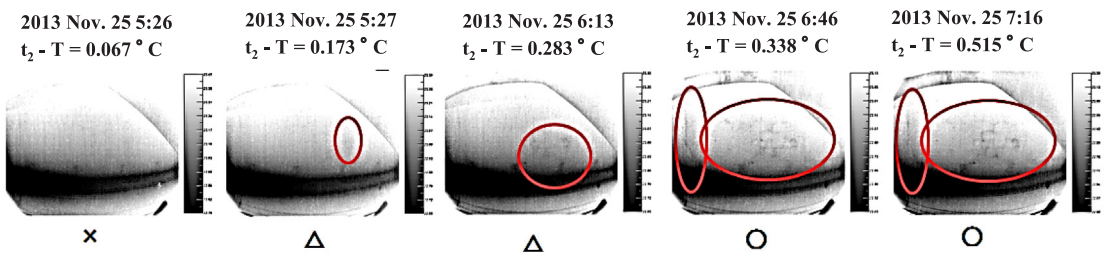

Fig. 7. Thermal images captured under the condition that the temperature difference between the concrete surface and the tunnel air is between 0 °C and 0.515 °C.

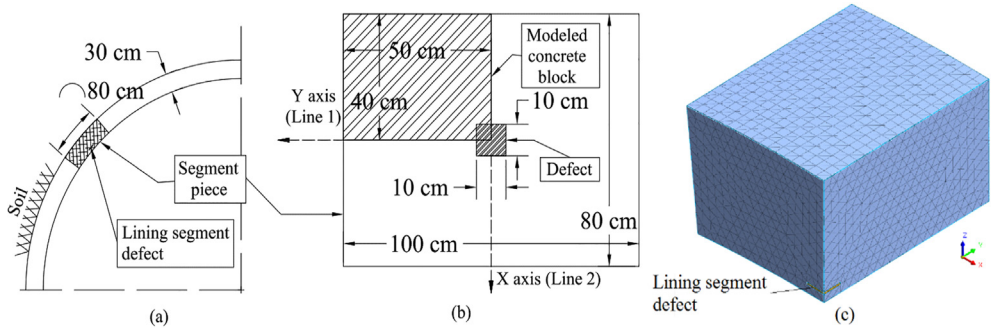

Fig. 8. (a) Tunnel lining, and segment defect, (b) modeled concrete block, and (c) analytical model of the segment piece.

Figs. 3 and 4. The cavity in the lining is located inside the surface at a depth of a few centimeters, and the heat transfer is likely to transfer through its surfaces via radiation. The initial temperature of the concrete segment is read from field data (for instance, 23.04 °C is set for ideal condition as shown in Fig. 3). The change in the time-dependent temperature on the surface of the concrete segment is an unknown variable.

Table 1 lists the input parameters of the numerical model. Among the thermal parameters of the concrete, the specific heat *c* and the thermal conductivity *k* depend on the temperature of the concrete (European 2, 1995). The specific heat of a normal concrete is affected by the moisture content, grain composition, and density of the concrete. Moreover, the thermal conductivity varies with the density and permeability of the concrete (Phan, 1996). For the analyses, the thermal conductivity and specific heat of the concrete are initially selected by referring to the range of thermal parameters of the normal concrete available in literature (European 2, 1995; Harmathy, 1970; Incropera, Frank and DeWitt, 1990). The heat transfer coefficient was derived by trial and error. The latter parameter was changed by introducing the variation in the field-measured tunnel air temperature (see Fig. 3) into the numerical model, and subsequently, monitoring the temperature changes on the healthy and unhealthy concrete surfaces with respect to time. The input parameters, listed in Table 1, were obtained after closely fitting the measurement data and numerical results, as shown in Fig. 9. According to Konishi et al. (2016) who also used the same measurement data as those used in this study, the average of the maximum steel bar corrosion in the measurement data was reported to be between 1.9 and 3 cm. The temperatures of the unhealthy and healthy surfaces obtained using the numerical analyses do not show that the temperature increases as much as that observed in the field measurement after approximately 8:30 AM. This implies that the concrete surface on the field is more sensitive to the change in the temperature compared to the numerical results. By employing the numerical modeling, this degree of sensitivity was unnoticeable.

The numerical fitting was performed assuming a void at the depth of 2 cm from the concrete surface with dimensions of 10 cm × 10 cm × 0.5 cm (length × width × thickness). The initial surface temperature of the concrete is 23.05 °C based on the measurement data shown in Fig. 3(a).

Fig. 10 shows the effect of considering the radiation in detecting the void. The figure shows that considering the radiation effect on the void leads to an increase in the rate of heat transfer, thereby increasing the temperature of the unhealthy concrete surface beyond that of the healthy concrete, which is not the case required for the measurement data. Hence, to have a better agreement between the analysis results and the measurement data, the radiation effect on the void is ignored in the numerical analyses.

3.3. Temperature changes on concrete-lining surface

Different recommendations have been given for the optimum time range for the IRT imaging of various structures. For instance, Hiasa et al. (2015) preferred nighttime for inspecting the concrete bridge deck as the temperature difference is more stable without any heat noises. The appropriate time for capturing the IRT images of the concrete lining of the tunnel is when the temperature difference between the tunnel air and the concrete surface becomes maximum. Based on the field data shown in Fig. 3, the tunnel air temperature decreases from 9 PM to approximately 8:30 AM, and subsequently, increases gradually up to 9 PM, and this cycle repeats daily. The increase in the tunnel air temperature is largely because trains start to run on the line. The trains halt between 1 AM and 5 AM, and during this time, the inspection of the tunnel is feasible. This time range is used to obtain the numerical results.

Fig. 11 shows the comparison between the field measurement, shown in Fig. 3(b), and the numerical results of the temperature difference between the concrete surface and the tunnel air ($t_2 - T$) and that between the unhealthy and healthy concrete surfaces ($t_2 - t_1$). The

Table 1
Input parameters used in the heat transfer analyses.

Input parameters (concrete)	Unit	Input values	Recommended value in literature (Reference)
Specific heat, c	J/kg K	1150	840–1170, (Harmathy, 1970)
Thermal conductivity, k	W/m K	0.5	0.5–3.3, (Liu et al., 2014)
Heat transfer coefficient, h	W/m^2 C	3	Derived by trial and error
Emissivity, e	–	0.92	0.88–0.93, (Bergman et al., 2011)
Thermal expansion coefficient, a	mm/mm	1×10^{-5}	(Eurocode 2, 1995)
Mass density, g	kg/m^3	2300	(Eurocode 2, 1995)
Stephan–Boltzmann constant, σ	$W/m^2 K^4$	5.67×10^{-8}	(Cengel, 2007)
Initial temperature	°C	23.04	(Field measurement)
Input parameters (air)	Unit	Input values	Value of parameter in literature (Reference)
Specific heat, c	J/kg K	1000	(Dixon, 2007)
Thermal conductivity, k	W/m K	0.021	(Dixon, 2007)
Thermal expansion coefficient, a	mm/mm	0.0034	(Dixon, 2007)
Mass density, g	kg/m^3	1.225	(Dixon, 2007)

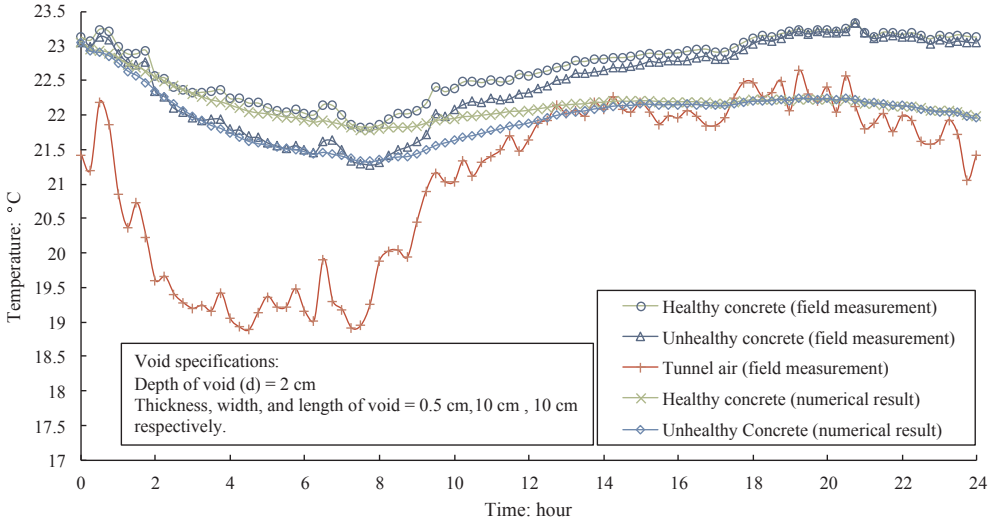

Fig. 9. Fitting of temperatures of healthy and unhealthy concrete surfaces between field measurements and numerical results.

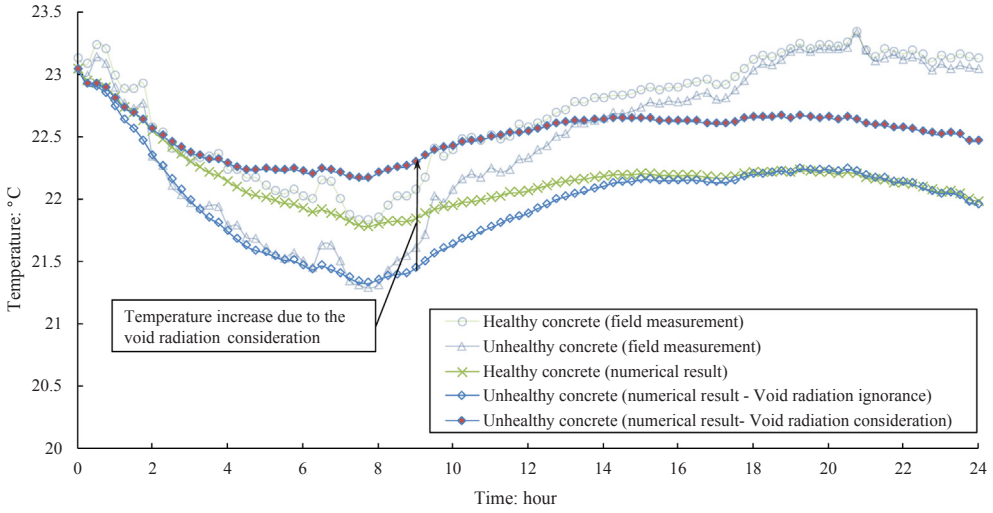

Fig. 10. Surface temperature of the unhealthy concrete with and without void radiation.

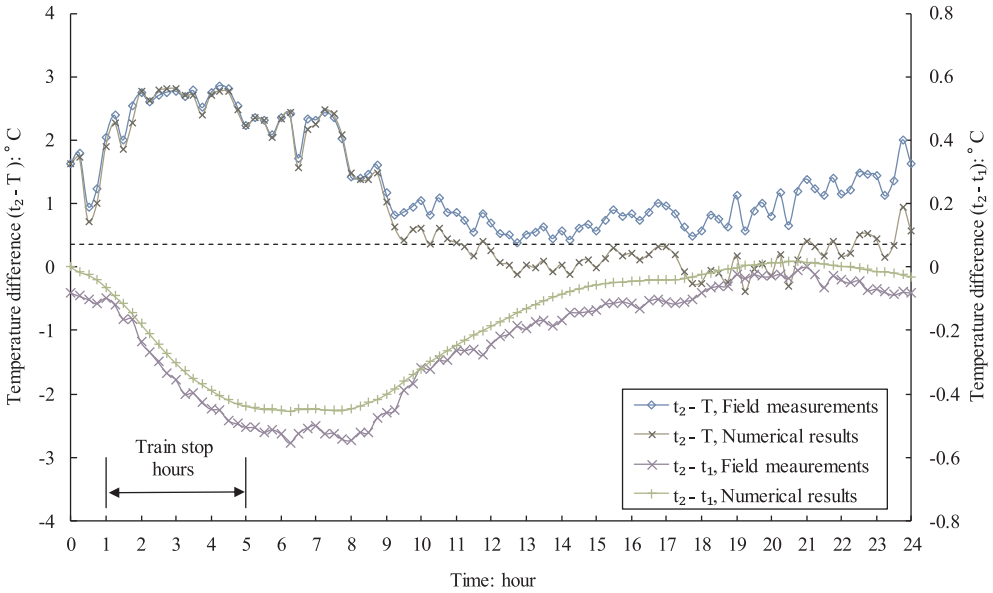

Fig. 11. Comparison of the temperature difference of the tunnel air and healthy and unhealthy concrete surfaces between field measurement and numerical analyses (ideal condition).

$t_2 - T$ values for the measurement data are more than 0.35 °C; this value for the numerical outputs is somewhat lower after 8:30 AM, which follows the pattern already explained in Fig. 10. The $t_2 - t_1$ values are between 0 °C and 0.55 °C in both the numerical results and field measurements. During the non-operating hours of the trains, this value is more than the camera detection threshold (ideal condition). Fig. 12 shows a comparison between the field data, shown in Fig. 4(b), and the numerical results of $t_2 - T$ and $t_2 - t_1$. Except for the time between approximately 7 to 9 AM, both the measurement data and numerical results show that the $t_2 - T$ values are less than 0.35 °C. The measured t_1 and therefore $t_2 - t_1$ data were only available until noon. Using the developed model, however, the analyses were extended such that the results could be presented for 24 h. The $|t_2 - t_1|$ values are limited to 0.15 °C in both the numerical results and field measurements. During the 24 h, these values are less than the camera detection threshold. This implies that it is difficult to detect defects on the concrete surface under this condition (difficult condition). Nevertheless, the numerical results for both the ideal condition (Fig. 11) and difficult condition (Fig. 12) are in good agreement with the measurement data.

Fig. 5 shows the variation in the temperature along the Line 1 (y axis) and line 2 (x axis) for a defected concrete surface. Fig. 13(a) and (b) show the numerical results of the normalized temperature variation on the concrete surface $T - T_{min}/T_{max} - T_{min}$ with respect to every hour during the non-operating hours of the trains. In these figures, the changes in the temperature for a distance of 10 cm from the center of the void along the y-axis, i.e., Line 1 and x-axis, i.e., Line 2, are shown. T_{max} and T_{min} are the maximum and minimum temperatures, respectively, of the unhealthy concrete surface obtained hourly during the non-operating hours of the trains (1 to 5 AM).

In Fig. 13(a) and (b), both the field measurement and numerical results signify the location of the void via the temperature difference around the void. As mentioned earlier, the temperature distribution along Line 1 is largely symmetrical; however, it decreases slightly along the positive direction of Line 2 because the temperature near the tunnel crown is higher. As the field data pertaining to the variation in the tunnel temperature with respect to the height were unavailable, the variation in the temperature on the concrete surface was considered constant with respect to the height, thus leading to a discrepancy between the numerical and measurement data, as shown in Fig. 13(b).

3.4. Open and closed cavities

The corrosion-induced cavities in the concrete lining of the tunnel can be divided into two types: if the cavity is in contact with the tunnel air, the cavity is termed *open*; otherwise, it is called *closed*, as shown in Fig. 14. In an open cavity, the temperature inside the cavity changes depending on the variation in the temperature of the tunnel air. Fig. 15 shows the numerical results of the temperature changes on the two unhealthy surfaces in the cases of the open and closed cavities.

The temperatures of the healthy concrete surface and tunnel air are also shown on the same graph. In the case of the open cavity, the cavity walls are affected by the outside air, and the temperature on the lining surface becomes closer to that of the tunnel air. Therefore, the lining surface in the case of the closed cavity exhibits a lower temperature compared to that in the open cavity type. This implies that while inspecting cavities with the same depth using IRT, the ones with a closed boundary can be easily detected. Fig. 16 shows the numerical result of the temperature distribution for the open and closed cavities at a time of 5 h.

3.5. Considerations of void depth and temperatures of healthy and unhealthy concrete surfaces and tunnel air

In this section, the temperature measurement data, shown in Fig. 4(a) and (b) are considered. This set of data was measured on November 25, 2013 along the RC box-type tunnel, and the tunnel air temperature values are close to that of the lining surface. The measurement data of t_1, and thus, $t_2 - t_1$ were available until 12 noon. As shown in Fig. 4(b), except for the time between approximately 7 and 9 AM, $t_2 - T$ values are less than 0.35 °C and $|t_2 - t_1|$ values are less than 0. 15 °C.

Based on the collected field measurements in this study, the voids due to the steel bar corrosion are located at a depth ranging from 19 mm to 30 mm. The infrared active thermometry is suitable for detecting defects in concrete structures when the void depth is less than 10 cm. However, it is recommended to set this limitation at a depth of 5 cm in the case of passive thermometry (Sakagami and Kubo, 2002).

By considering the data pertaining to the tunnel air temperature, shown in Fig. 4, between 12 midnight to 12 noon, the void depth was changed between 5 and 50 mm to monitor its influence on the temperatures of the healthy and unhealthy lining surfaces. Fig. 17(a) and (b) show the numerical results of the void depth effect on $t_2 - t_1$ and

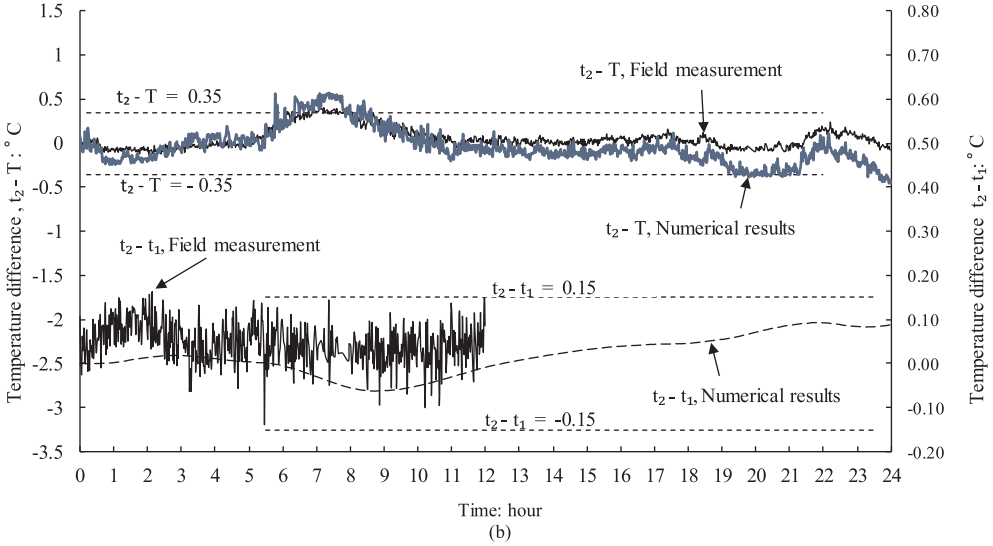

Fig. 12. Comparison of the temperature difference of the tunnel air and healthy and unhealthy concrete surfaces between field measurement and numerical analyses (difficult condition).

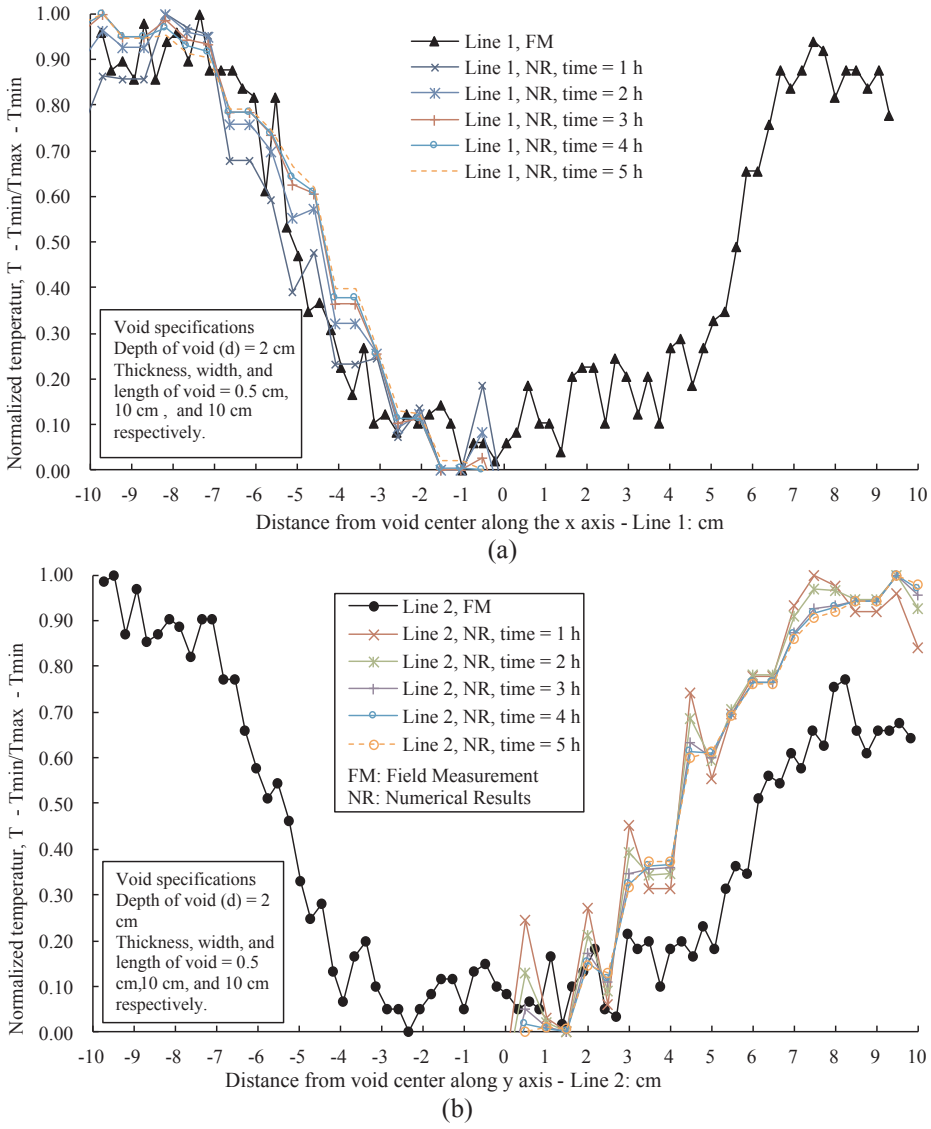

Fig. 13. Normalized temperature variation along the x axis: Line 1 (a) and y axis: Line 2 (b) (Lines 1 and 2 are shown in Fig. 5).

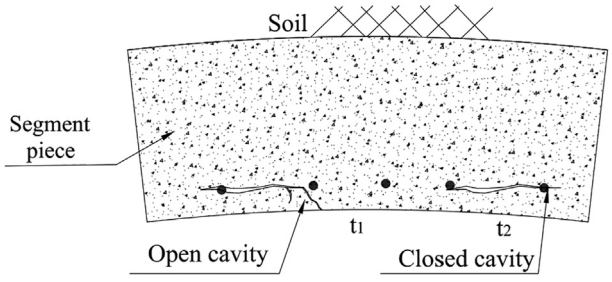

Fig. 14. Open and closed types of cavities.

$t_2 - T$, respectively.

To obtain the data, shown in Fig. 17(a), the void depth was varied, and the values of $t_2 - t_1$ were calculated between 12 midnight to 12 noon. The maximum and minimum values of $t_2 - t_1$ were observed at times of 1 AM and 7:30 AM, respectively. The sensitivity threshold of the temperature difference obtained using the camera ($|t_2 - t_1| = 0.03$) was also shown in the graph. By increasing the void depth, $t_2 - t_1$ becomes smaller and the chances of detecting the voids decrease. The data are quite informative, e.g., for a time ranging approximately from 7 to 9 AM, the $t_2 - t_1$ values with respect to the depth of the void can be represented to that obtained at a time of 7:30 AM as shown in Fig. 17(a). For this time limit, the voids with depths less than 30 mm are detectable using the camera as $t_2 - t_1 > 0.03$ °C. Moreover, beyond this time limit, say 1 AM, the voids with a depth of 13 mm or less are detectable.

Fig. 17(b) shows that the variation in $t_2 - T$ with respect to the void depth is not so sensitive. For depths more than 30 mm, the variation in $t_2 - T$ is largely independent of the depth, whereas it gradually decreases for depths under 30 mm. This implies that in the case of shallow voids, as the defected portion of the lining surface is small, the temperature on the surface quickly becomes in equilibrium with the tunnel air temperature, and thus, approaches the same more faster compared to that observed for deeper voids. The maximum value of $t_2 - T$ occurs at 7:30 AM, as shown in Fig. 17(b). $t_2 - T$ is greater than 0.35 °C for a time limit ranging from 7 to 9 AM whereas it is < 0.35 °C for other times, which closely matches with the field measurement data, as shown in Fig. 4(b). Therefore, a temperature difference between the concrete surface and the tunnel air of more than 0.35 °C, i.e., $t_2 - T > 0.35$ °C, is an ideal condition for detecting the voids with an approximate depth of 30 mm or less.

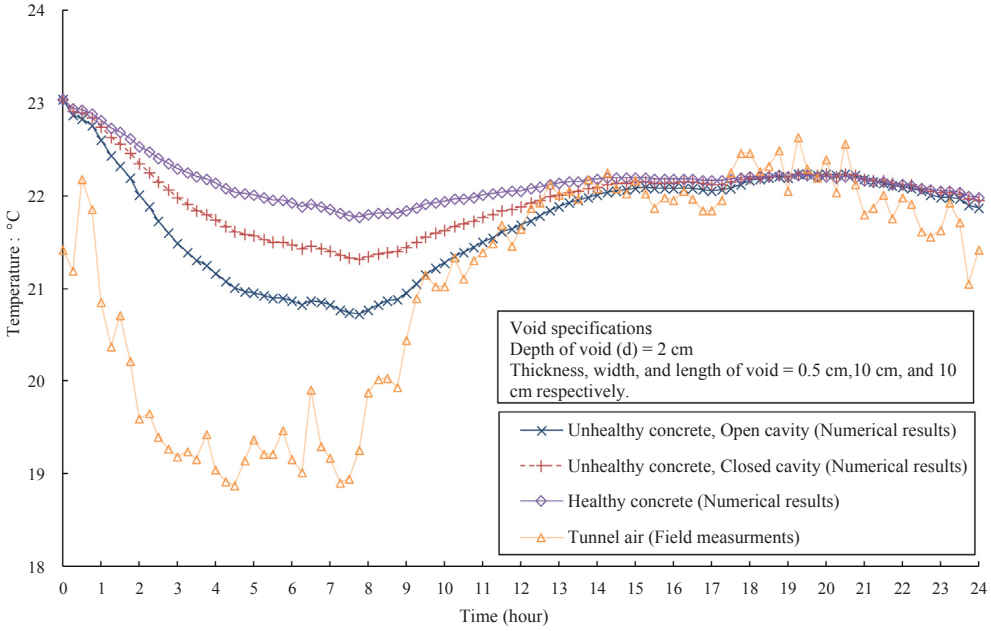

Fig. 15. Temperature variation on the lining surfaces of the open and closed cavities with respect to the changes in the tunnel air temperature.

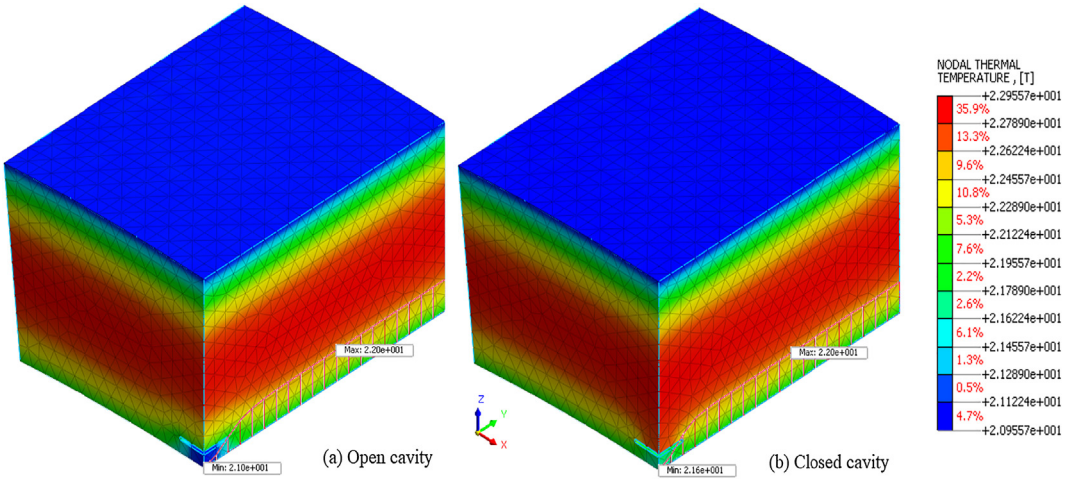

Fig. 16. Numerical results of the temperature distribution for the open and closed cavities at time = 5 h using the data shown in Fig. 3.

4. Conclusion

This study simulated the defect detection of an unhealthy part of a tunnel concrete lining using field temperature measurements and numerical analyses. A model of the heat transfer in the concrete, tunnel air, and air inside the defected part of the concrete was employed by considering heat transfer mechanisms, and subsequently, validating the same by comparing with field measurements. The normalized temperature distribution on the concrete surface around a void was shown. Two types of cavities were considered discussed, and the effects of void depth on the temperatures of the healthy and unhealthy lining surfaces were investigated.

The following are the main findings of this study:

1. The normalized temperature distribution on the concrete surface along the two perpendicular lines of a defected part of the unhealthy concrete in the case of the RC box-type tunnel was used to detect the location of the defects. The numerical results of the normalized temperature curve around the defected part is similar to the results of the field measurement along Line 1; however, along Line 2, a discrepancy was observed between the measurement and numerical results as the field data pertaining to the variation in tunnel temperature with respect to the height were unavailable. By accessing these types of field data, a better surface temperature fit between the numerical results and measurement data along the two perpendicular lines is possible.
2. Two types of corrosion-induced cavities were discussed: open and closed. In the case of the open cavity, the cavity walls are affected by the outside air, and the temperature on the lining surface becomes closer to that of the tunnel air. The lining surface in the case of the closed cavity exhibits a lower temperature compared to the open-cavity type. This implies that while detecting cavities with the same depth using the surface-temperature differences, the ones with the closed boundary could be easily detected. The studied cavities were parallel to the concrete surface; however, cavities with different alignment angles with respect to the concrete surface could be investigated in the future.
3. By increasing the void depth, the temperature difference between the healthy and unhealthy concrete surfaces becomes smaller, thereby decreasing the chances of detecting the voids. The

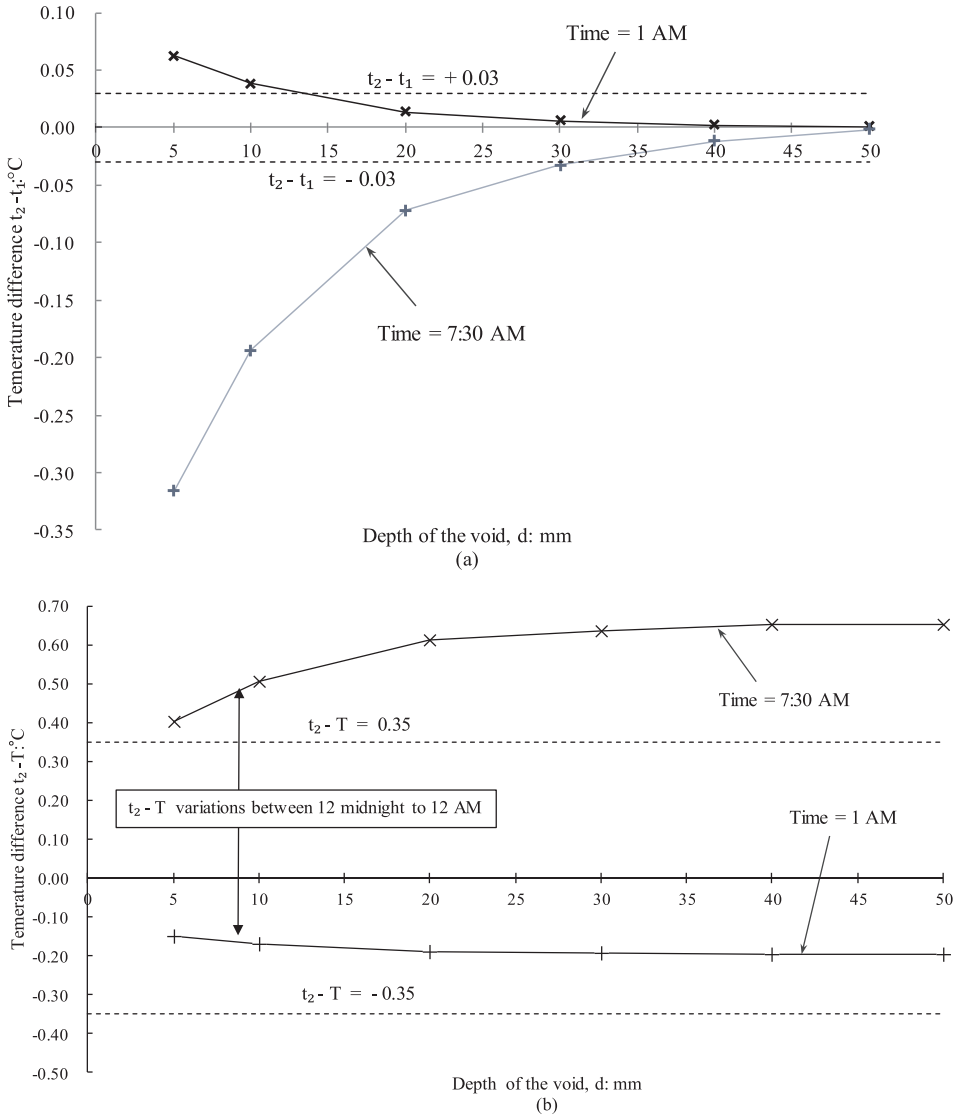

Fig. 17. Numerical results of void depth effect on the variations in (a) $t_2 - t_1$, and (b) $t_2 - T$.

numerical results show that the temperature difference between the healthy and unhealthy concrete surfaces, i.e., $t_2 - t_1$, depends on both the void depth and the temperature difference between the concrete surface and the tunnel air, i.e., $t_2 - T$. During performing of infrared thermometry, as the temperature difference between the tunnel air and the concrete surface becomes greater, deeper voids can be detected.

4. The temperature difference between the tunnel air and the defected concrete surface is not so sensitive to the void depth. For void depths more than 30 mm, this temperature difference is largely independent of the depth. A temperature difference between the concrete surface and the tunnel air of more than 0.35 °C, i.e., $t_2 - T > 0.35$ °C, is an ideal condition for detecting voids with an approximate depth of 30 mm or less.

Appendix A. Supplementary material

Supplementary data to this article can be found online at https://doi.org/10.1016/j.tust.2019.01.013.

References

Bergman, T.L., Incropera, F.P., DeWitt, D.P., Lavine, A.S., 2011. Fundamentals of heat and mass transfer. John Wiley & Sons.
Cengel, Y.A., 2007. Heat and Mass Transfer: A Practical Approach. 2007. McGraw-Hill Education. https://doi.org/10.1017/CBO9780511676420.004.
Danesi, S., Salerno, A., Wu, D., Busse, G., 1998. Cooling down thermography: principle and results for NDE 266–274. https://doi.org/10.1117/12.304736.
Dixon, J.C., 2007. Appendix B: Properties of Air. In: The Shock Absorber Handbook. Wiley Online Library, pp. 375–378.
European Committee, 1995. Eurocode 2, Design of concrete structures - Part 1-2: General rules-Structural fire design.
Guo, L., Guo, L., Zhong, L., Zhu, Y., 2011. Thermal conductivity and heat transfer coefficient of concrete. J. Wuhan Univ. Technol. Mater. Sci. Ed. 26, 791–796. https://doi.org/10.1007/s11595-011-0312-3.
Harmathy, T., 1970. Thermal properties of concrete at elevated temperatures. J. Mater. 5, 47–74.
Hiasa, S., Watase, A., Birgul, R., Matsumoto, M., Mitani, K., Catbas, N., 2015. Utilizing Infrared technologies as a non-destructive evaluation for maintenance of concrete structures. Life-Cycle Struct. Syst. Des. Assessment, Maint. Manag. CRC Press Boca Raton, FL, USA, pp. 598–605.
Holman, J.P., 1990. Heat Transfer. McGraw-Hill Inc, New York.
Frank, P.I., DeWitt, D.P., 1990. Fundamentals of Heat and Mass Transfer, 1985. John Wiley and Sons.
Kim, J.J., Youm, K.S., Reda Taha, M.M., 2014. Extracting concrete thermal characteristics from temperature time history of rc column exposed to standard fire. Sci. World J. 2014, 22–24. https://doi.org/10.1155/2014/242806.
Konishi, S., Kawakami, K., Taguchi, M., 2016. Inspection method with infrared thermometry for detect void in subway tunnel lining. Procedia Eng. 165, 474–483. https://doi.org/10.1016/j.proeng.2016.11.723.
Kyuma, K., 1985. Soil temperature regime of Japanese soils. Soil Sci. Plant Nutr. 31, 463–468.
Liu, M.Y.J., Alengaram, U.J., Jumaat, M.Z., Mo, K.H., 2014. Evaluation of thermal

conductivity, mechanical and transport properties of lightweight aggregate foamed geopolymer concrete. Energy Build. 72, 238–245. https://doi.org/10.1016/j.enbuild.2013.12.029.
Mahmoud, A.M., Ben-Nakhi, A., Ben-Nakhi, A., Alajmi, R., 2012. Conjugate conduction convection and radiation heat transfer through hollow autoclaved aerated concrete blocks. J. Build. Perform. Sim. 5, 248–262.
Maierhofer, C., Arndt, R., Röllig, M., Rieck, C., Walther, A., Scheel, H., Hillemeier, B., 2006. Application of impulse-thermography for non-destructive assessment of concrete structures. Cem. Concr. Compos. 28, 393–401. https://doi.org/10.1016/j.cemconcomp.2006.02.011.
Maierhofer, C., Wiggenhauser, H., Brink, A., Röllig, M., 2004. Quantitative numerical analysis of transient IR-experiments on buildings. Infrared Phys. Technol. 46, 173–180. https://doi.org/10.1016/j.infrared.2004.03.022.
Mydin, M.O., 2013. Modeling of transient heat transfer in foamed concrete slab. J. Eng. Sci. Tech. 8, 326–343.
Phan, L.T., 1996. Fire performance of high-strength concrete: A report of the state-of-the art. US Department of Commerce, Technology Administration, National Institute of Standards and Technology, Office of Applied Economics, Building and Fire Research Laboratory.
Sakagami, T., Kubo, S., 2002. Development of a new non-destructive testing technique for quantitative evaluations of delamination defects in concrete structures based on phase delay measurement using lock-in thermography. Infrared Phys. Technol. 43, 311–316. https://doi.org/10.1016/S1350-4495(02)00157-3.
Scott, M., Luttig, H., Strydom, M., Gonelli, M., Kruger, D., Rankine, R.G.D., Broodryk, T., 2012. Passive infrared thermography as a diagnostic tool in civil engineering structural material health monitoring. CRC Press, pp. 274.
Showunmi, T., 2013. Finite element infrared thermography study on concrete and steel-concrete composite structures.